Computer-Aided Multiview Tumor Detection for Automated Whole Breast Ultrasound

Chiao Lo[1], Yi-Wei Shen[2], Chiun-Sheng Huang[1,3], and Ruey-Feng Chang[2]

Abstract

Automated whole breast ultrasound (ABUS) has become a popular screening tool in recent years. To reduce the review time and misdetection from ABUS images by physicians, a computer-aided detection (CADe) system for ABUS images based on a multiview method is proposed in this study. A total of 58 pathology-proven lesions from 41 patients were used to evaluate the performance of the system. In the proposed CADe system, the fuzzy c-mean clustering method was applied to detect tumor candidates from these ABUS images. Subsequently, the tumor likelihoods of these candidates could be estimated by a logistic linear regression model based on the intensity, morphology, location, and size features in the transverse, longitudinal, and coronal views. Finally, the multiview tumor likelihoods of the tumor candidates could be obtained from the estimated tumor likelihoods of the three views, and the tumor candidates with high multiview tumor likelihoods were regarded as the detected tumors in the proposed system. The sensitivities of the multiview tumor detection for selecting 5, 10, 20, and 30 tumor candidates with the largest multiview tumor likelihoods were 79.31%, 86.21%, 96.55%, and 98.28%, respectively.

Introduction

Breast cancer is the most frequently diagnosed cancer in women and is the second leading cause of cancer among women in the United States.[1] In recent years, the mortality rates of breast cancer have been reduced because of improved treatment and early detection methods.[2]

Mammography is the standard screening tool for breast cancer detection.[3-5] However, mammography sensitivity declines in women with denser breasts.[6,7] Women with dense breasts have

[1]Department of Surgery, National Taiwan University Hospital, Taipei, Taiwan
[2]Department of Computer Science and Information Engineering, National Taiwan University, Taipei, Taiwan
[3]Department of Surgery, National Taiwan University College of Medicine, Taipei, Taiwan

Corresponding Author:
Ruey-Feng Chang, Department of Computer Science and Information Engineering, National Taiwan University, Taipei 10617, Taiwan.
Email: rfchang@csie.ntu.edu.tw

higher risks of breast cancer than those with less dense breasts.[8,9] Breast ultrasound (US) has emerged as the most important adjunct to mammography.[10,11] Several studies[6,12-16] have proposed that the use of US for screening women with dense breasts could improve the accuracy of breast cancer detection. However, the accuracy of the traditional hand-held US devices are operator dependent, and the results are poorly reproducible and slow.[12,13] To overcome these disadvantages, automated breast US (ABUS) devices have been introduced and investigated in recent years.[13,14,17-20] The ABUS images are acquired by a motor-driven transducer, which scans breasts automatically. ABUS devices are operator independent, and the results are reproducible.[21] However, physicians still require a significant amount of time to review hundreds of images acquired by ABUS. To reduce the reviewing time, computer-aided detection (CADe) systems could be utilized.

In recent years, few proposed studies have used the CADe system for ABUS image analysis.[13,22] In a study by Ikedo et al.,[13] edge and density parameters were applied toward lesion detection, and the watershed algorithm was adapted to segment suspicious lesions. To reduce the number of false positives (FPs), a quadratic discriminant analysis was applied to distinguish tumors and FPs from the segmented suspicious lesions. The sensitivity of the CADe system was 80.6% with 3.8 FPs per whole breast image. Chang et al.[22] used a CADe system with a gray-level slicing method to segment suspicious lesions; seven features were used to distinguish the lesions and nontumors from all suspicious lesions. The sensitivity of the CADe system was 92.3% with 1.76 FPs per case.

The fuzzy-c-mean (FCM) algorithm has been used in the medical imaging segmentations[23-26] because it could cluster data according to data distribution without user bias. In this study, the FCM algorithm was adopted to detect the tumor candidates from the ABUS images. However, both lesions and many nontumors were identified as tumor candidates. To reduce the FPs of the CADe system, the intensity, morphology, location, and size features were measured and the tumor likelihoods of these tumor candidates were estimated using a linear regression model[27] of these parameters. All aforementioned procedures used in this study were performed in two-dimensional (2D) space. Because ABUS images were constructed from three orthogonal views (transverse, longitudinal, and coronal views), these procedures were applied to the three views. Finally, the estimated tumor likelihoods of the tumor candidates in the three orthogonal views were combined to obtain the multiview tumor likelihoods of the tumor candidates. The tumor candidates with high multiview tumor likelihoods were considered the detected lesions by the CADe system.

Materials and Method

Data Acquisition

In this study, the ABUS images were collected from the Breast Center of National Taiwan University Hospital and were acquired by an ABUS machine SomoVu ScanStation (U-System, Inc., San Jose, CA, USA) from November 2005 to June 2006. There were a total 58 lesions in 41 patients from the acquired ABUS images. Pathological assays with US-guided core needle biopsies (size range: 0.5-5.2 cm; $M \pm SD$: 1.81 ± 1.25 cm) revealed 36 malignant lesions and 22 benign lesions. The malignant lesions included 1 ductal carcinoma in situ (DCIS), 1 invasive papillary carcinoma, and 34 invasive ductal carcinomas (IDCs). The benign lesions included 13 fibrocystic changes, 7 fibroadenomas, 1 intraductal papilloma, and 1 granulomatous mastitis. For this study, approval was obtained from our institutional review board and informed consent was waived.

The SomoVu ScanStation scans over a breast with a 10 MHz linear transducer to obtain approximately two hundred 2D US images on each pass. The 15.4 cm transducer width is wider

than other conventional US probes, and only two or three passes were required to completely scan a whole breast. During the examination, the patient is in the supine position as the ABUS images are automatically acquired. The images of each scan are stored into a file. The file is decomposed into serial 2D US 512×743 pixel images at resolutions of 1.6 pixels/mm in the transverse, 3.5 pixels/mm in the longitudinal, and 14.9 pixels/mm in the coronal directions. The transverse, longitudinal, and coronal views of whole breast US could be obtained through the reconstruction of these 2D images.

To reduce the processing time of tumor detection, a subsampling method was adopted. In this procedure, we defined three parameters mer_t, mer_l, and mer_c to represent the number of US images that would be overlapped in the transverse, longitudinal, and coronal views, respectively. For example, if we define the parameter $mer_t = 10$ and assume that the variable $images\_Num_t$ is the number of original images in the transverse direction, a composite image is overlapped for every 10 images in the transverse direction; the number of composite images in the transverse direction is then $images\_Num_t/mer_t$. In this article, $mer_t = 7$, $mer_l = 7$, and $mer_c = 5$. Because breast tumors generally appear darker (i.e., lower intensity) than the surrounding normal tissue in US images,[28] the minimum and the mean values are usually adopted to perform the overlapping procedure. There are some lesions with partial dark inside in ABUS images. To avoid misdetection in these lesions, we adopt the minimum value as the overlapped result rather than the mean value in the procedure. It should be noted that using minimum value as the overlapped result might introduce a false bias.

Multiview Tumor Detection for Automated Whole Breast Ultrasound Imaging

In this section, multiview tumor detection in ABUS images will be introduced; the flowchart is shown as Figure 1. After overlapping the original data, the images were preprocessed using the sigma[29] and stick[30,31] filters to improve the image quality. Next, the tumor candidate regions were detected by FCM clustering. However, there were many FPs in the tumor candidates after candidate segmentation. To distinguish the tumors and FPs from the tumor candidates, the intensity, morphology, location, and size features were extracted, and the tumor likelihoods of the tumor candidates were estimated using linear regressions [27] of these parameters in each orthogonal view. Finally, multiview tumor likelihoods were obtained from the tumor likelihoods in each of the three orthogonal views. The tumor candidates were regarded as detected tumors in the CADe system if their multiview tumor likelihoods were greater than a specific threshold.

Preprocessing techniques. A strong speckle was present in the US images[32,33] because of wave interference inherent in coherent imaging process.[34] The speckle reduces the image quality and complicates object extraction and feature analysis.[35,36] Several conventional low-pass filters, such as the averaging filter,[37] can be used to reduce the speckle. However, texture patterns and boundary information are also blurred after applying these low-pass filters. It is difficult to detect and extract tumors in US images without the edge information. The sigma filter[29] was adopted in this study to reduce the speckle and retain the edge information.

Enhancing the region boundary could improve tumor detection performance.[38] The stick filter[30,31] was used to enhance the contrast of the edges for extracting the boundary information. In this study, a stick with a size of 7×7 square area was adopted to enhance the edge information, and 12 templates with short lines of possible orientations were adopted in the stick processing. Figure 2 shows an example of a 2D image before processing (Figure 2a) and the result after applying the sigmoid and stick filters to original image (Figure 2b).
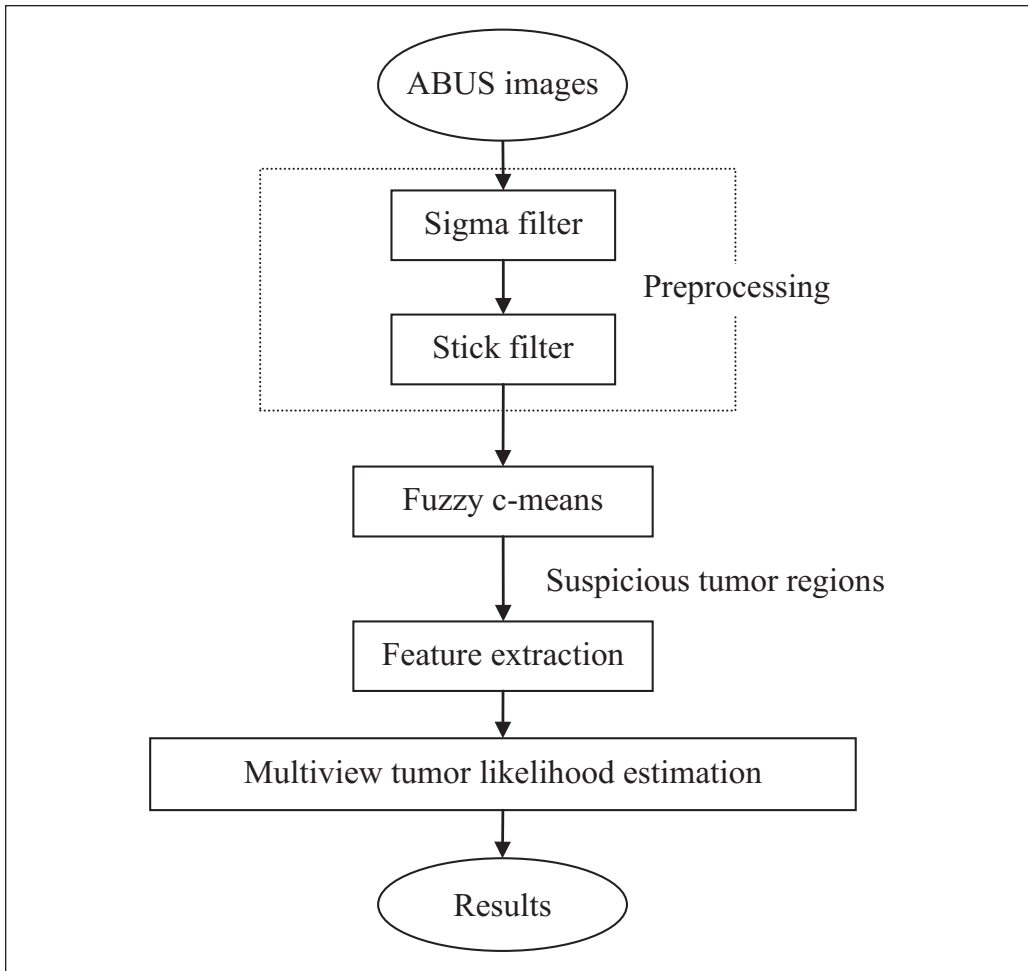
Figure 1. The flowchart of the multiview tumor detection system.

Tumor candidate detection. The FCM algorithm classifies image pixels according to intensity distribution. It uses a suitable threshold for automatic tumor candidate detection thereby removing human bias. The echogenicity of breast US images can be categorized as hyperechoic, median echogenic, or hypoechoic structures [39]; the echogenicity of lesions in US images is typically hypoechoic. In this study, pixels classified in the darkest group were regarded as suspicious tumor pixels. These pixels were further classified into four groups to avoid tumor oversegmentation. The results of FCM clustering are shown in Figure 2(c). Finally, a connected component labeling process[40] was adopted to group the suspicious tumor pixels into tumor candidate regions for feature extraction.

Feature extraction. In the tumor candidate detection, the tumor candidate regions were detected by FCM clustering based on intensity values. However, clustering produced many nontumors in the tumor candidate regions. To decrease the FPs in the tumor candidate regions, the intensity, morphology, location, and size features were extracted to estimate the tumor likelihoods of these regions using a logistic regression model. The estimated tumor likelihood represents the
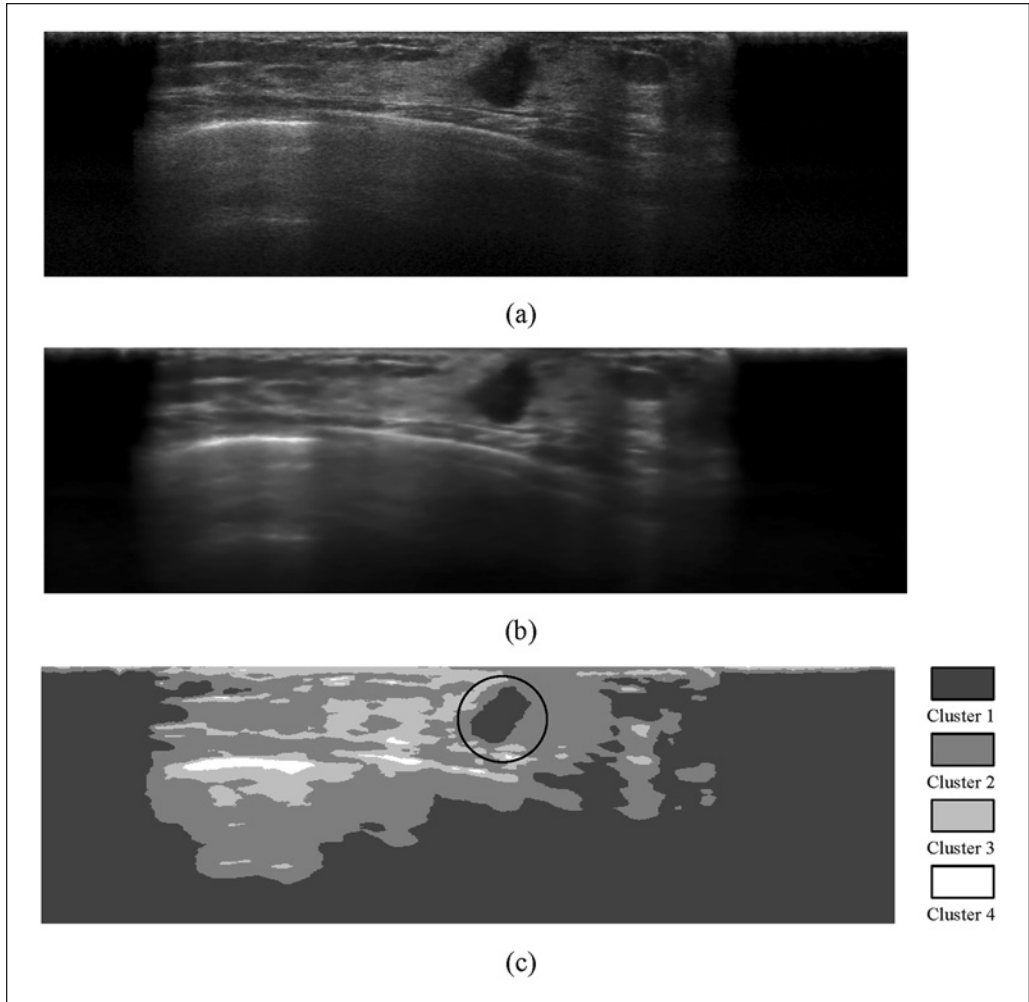
Figure 2. (a) Original image. (b) The result after applying the sigma and stick filters to (a). (c) The result generated by FCM clustering. The regions classified as the darkest group (Cluster 1) are regarded as tumor candidates and the tumor is indicated by the circle. FCM = fuzzy-c-mean.

probability that a tumor candidate is a lesion. The tumor candidates with tumor likelihoods that were greater than a specific threshold were regarded as detected lesions in the CADe system.

Intensity features. Because the intensities of breast tumors in US images were darker than those of the surrounding tissue, several intensity features could be used to aid in distinguishing tumors from nontumors. These features which include the intensity mean and standard deviations and the gradient intensity mean and standard deviations were extracted. In addition, the intensity difference between the outer and inner tumor candidate regions was calculated as follows:

$$\text{mean\_diff}_{out\_inner} = \text{mean}_{outer} - \text{mean}_{inner}, \tag{1}$$

where mean_{outer} is the mean intensity of the tumor candidate outer region and mean_{outer} is the mean intensity of the tumor candidate inner region. The tumor candidate outer region is a
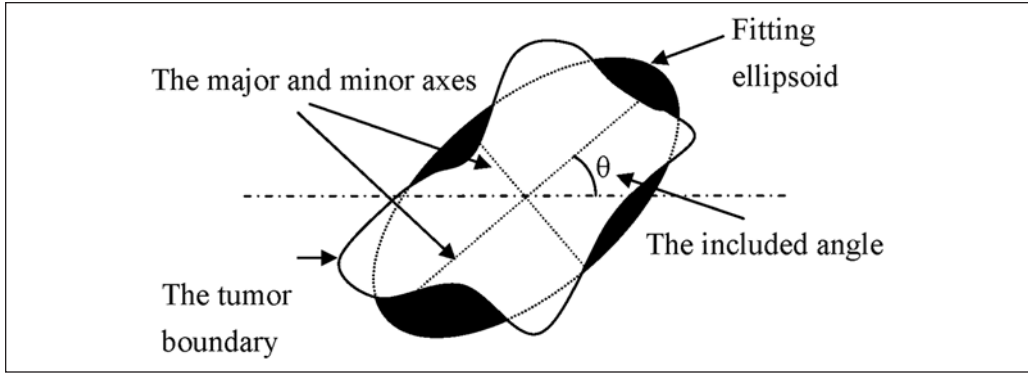
Figure 3. The tumor region and the fitting ellipsoid.

three-pixel width region extending outward from the segmented tumor candidate boundary. The tumor candidate inner region is a three-pixel width region extending inward from the segmented tumor candidate boundary.

Morphology features. Morphology features could be used to filter out the regions with abnormal morphology not similar to tumor shapes. In this study, the ellipse model[41] was evaluated with each tumor candidate. Morphology features were calculated by using the fitting ellipse model. The axis ratio ER_{axis} is defined as

$$ER_{\text{axis}} = \frac{L_2}{L_1}, \tag{2}$$

where L_1 and L_2 are the lengths of the major and minor axes of the fitting ellipse, respectively. The feature ER_{angle} is the angle between the major axis of the fitting ellipsoid and the horizontal axis (see Figure 3). The ratios ER_{inner} and ER_{outer} measure the similarity between the fitting ellipsoid and the tumor candidate regions and are defined as

$$ER_{\text{inner}} = \frac{A_{\text{tumor}} \bigcap A_E}{A_{\text{tumor}}} \quad \text{and} \tag{3}$$

$$ER_{\text{outer}} = \frac{A_{\text{tumor}} \bigcap \overline{A_E}}{A_{\text{tumor}}}, \tag{4}$$

where A_{tumor} is the area of the tumor candidate and A_E is the area of the fitting ellipsoid. Figure 4 indicates the inner and outer regions of the fitting ellipsoid. The compactness feature[42] is also calculated:

$$C_d = \frac{n - P/4}{n - \sqrt{n}}, \tag{5}$$

where n is the number of pixels in a tumor region and P is the perimeter of the tumor candidate region.

Location and size features. In addition to the intensity and morphology features, the location and size features were also used to detect breast lesions in US images. First, the size feature was used to exclude small noise and large objects. Second, because the rib region in US images is
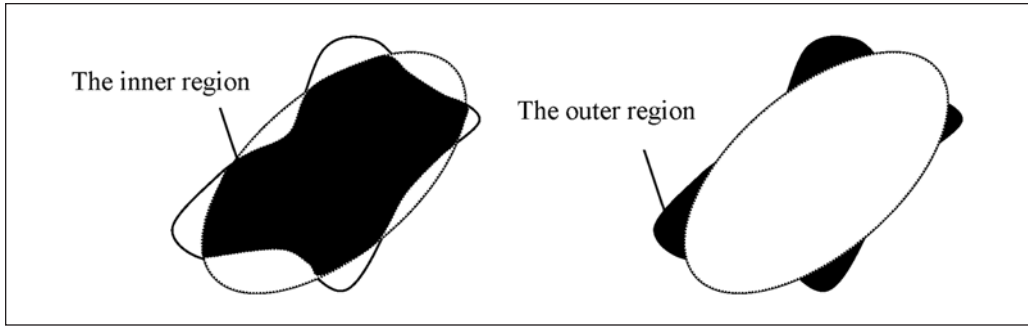
Figure 4. The inner and outer regions of the fitting ellipsoid.

hypoechoic and its shape is similar to a breast lesion, the rib region might be classified as a lesion using only intensity and morphology features. However, the thickness between skin and the rib region is greater than the thickness of breast tumors; by accounting for these location features, the rib regions are excluded from tumor candidates. Finally, breast lesions are usually visible in neighboring slices. This property was adopted in this study to improve detection reliability. The neighboring suspicious tumor feature is defined as follows:

$$NS(s) = \frac{N_{ta}}{N_{\text{tumor}}}, \tag{6}$$

where N_{tumor} is the pixel number of the tumor candidate region and N_{ta} is the number of pixels adjacent to the pixels of tumor candidate images.

Multiview tumor likelihood estimation. To detect lesions from tumor candidates, the tumor likelihoods of tumor candidates were estimated by a linear regression model.[27] The tumor candidate with a higher tumor likelihood is considered as a lesion. Because some features might have less information required for classification, a backward feature elimination [43] method was adopted to focus on the more important features without reducing the detection performance. In backward feature elimination, the tumor candidates of all cases were randomly partitioned into approximately equal training and testing sets. Initially, all features were included in the feature subset. A logistic regression model based on all features of the training set and the trained model was used to evaluate the performance of the testing set. The feature with the lowest classification ability in the testing set was removed from the feature subset. Then, the procedure was repeated until the difference of the residual sum of the squares of the classified results with and without the removed feature was not statistically significant. The features with the best performance of classifying lesions and nonlesions were selected as the important features. Subsequently, a binary logistic regression model with a 10-fold cross-validation [44] was adopted in the estimation of tumor likelihood. All tumor candidates were partitioned into 10 groups with approximately equal size. The tumor candidates of one group were included in the testing set and the tumor candidates of the other groups were used to formulate the logistic regression model. The tumor likelihoods of the tumor candidates in the testing set were predicted by the trained model. This procedure was repeated until all groups were evaluated. It should be noted that the feature selection was initially performed with all data; subsequent cross-validation was performed with the same data with a potential bias in the evaluated results.

The tumor likelihoods of all orthogonal views were combined to achieve better tumor detection accuracy. The estimated tumor likelihood of a tumor candidate is the probability that the candidate
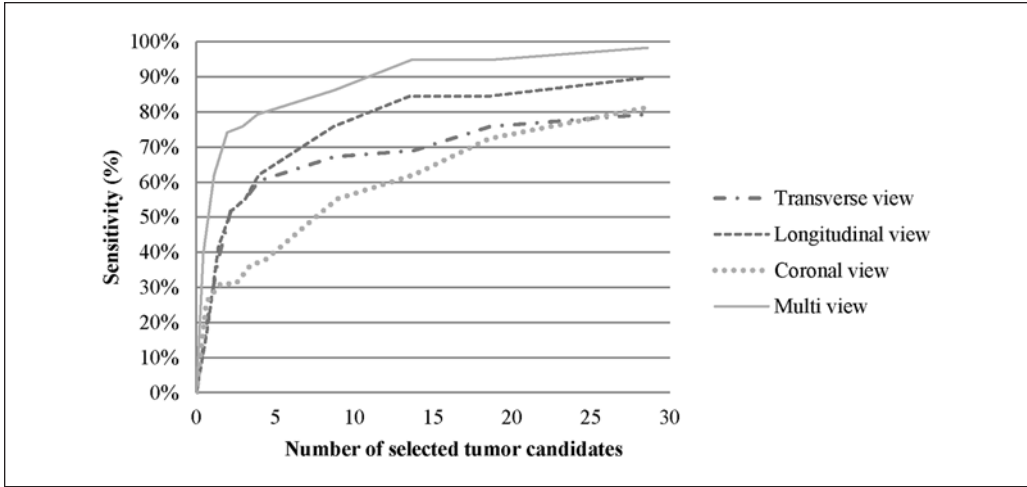
Figure 5. The FROC curves of the proposed system with single view and multiview with all features. FROC = free-response operating characteristics.

is a lesion. The 2D image slices of the three orthogonal views were used to reconstruct a 3D image. Based on our assumptions, the tumor likelihood of each pixel in one tumor candidate is the same as the estimated tumor likelihood of the tumor candidate in one orthogonal view. A multiview tumor candidate is the intersection region from the tumor candidates of each of the three views. The multiview tumor likelihood of each pixel of a multiview tumor candidate can be estimated as follows:

$$P_M\left(i,j,k\right) = \frac{P_T\left(i,j,k\right) + P_L\left(i,j,k\right) + P_C\left(i,j,k\right)}{3}, \tag{7}$$

where P_T, P_L, and P_C are the estimated tumor likelihoods of the pixel in the transverse, longitudinal, and coronal views, respectively. Finally, the multiview tumor likelihood of each multiview tumor candidate could be estimated as

$$P_{tc}\left(i,j,k\right) = \max_{(i,j,k)\in tc}\left\{P_M\left(i,j,k\right)\right\}, \tag{8}$$

where P_{tc} represents the estimated multiview tumor likelihood.

To evaluate the performance of the CADe system, the tumor candidates of one case were ranked by their tumor likelihoods and the N tumor candidates with the largest likelihoods were regarded as detected lesions. The free-response operating characteristic (FROC) [45] curves were adopted to evaluate the performance of the tumor detection system, and the N tumor candidates with the largest likelihoods were adjusted to generate the FROC curves. In the experiments, a total of 58 lesions in 41 patients were examined to verify the performance of the multiview tumor detection. Because three ABUS images were acquired to cover a whole breast of each patient, only one ABUS image with one or more visible lesions of each patient was included in the database to evaluate the proposed CADe system.

Results

The FROC curves with a single- or multiview tumor detection system using all the features were compared as shown in Figure 5. In the transverse view, the tumor detection sensitivities for N
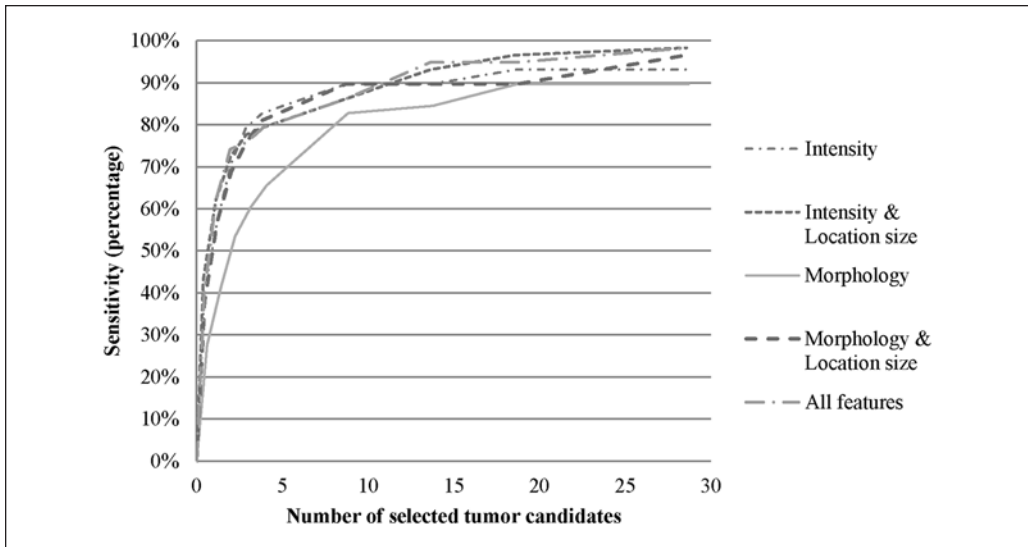
Figure 6. The FROC curves of the proposed system with multiview using different feature sets. FROC = free-response operating characteristics.

tumor candidates with the largest likelihoods were 60.34% ($N = 5$), 67.24% ($N = 10$), 75.86% ($N = 20$), and 79.31% ($N = 30$). In the longitudinal view, the tumor detection sensitivities were 62.07% ($N = 5$), 75.86% ($N = 10$), 84.48% ($N = 20$), and 89.66% ($N = 30$). In the coronal view, the tumor detection sensitivities were 37.93% ($N = 5$), 55.17% ($N = 10$), 72.41% ($N = 20$), and 81.03% ($N = 30$). The sensitivities in the multiview were 79.31% ($N = 5$), 86.21% ($N = 10$), 94.83% ($N = 20$), and 98.28% ($N = 30$). In Figure 6, the FROC curves with different feature sets were compared. When using the intensity and the location size features, the sensitivity was higher than that when using the other feature sets. The following analysis was adopted using the intensity and location size features. The sensitivity of tumor detection was 98.28% when selecting 30 tumor candidates with the largest likelihoods per case. The sensitivities of tumor detection for benign/malignant tumors are listed in Table 1. The sensitivities of tumor detection for benign and malignant tumors were 100% and 97.22%, respectively, when selecting 30 tumor candidates with the largest likelihoods per case. The sensitivities of tumor detection with different tumor sizes were also analyzed as listed in Table 2. Examples of the detected results are shown in Figures 7 and 8.

Discussion

Due to a large amount of data in an ABUS image, detecting suspicious lesions in the ABUS image is difficult and time-consuming. A CADe system could be used to assist physicians to improve the detection rate.[36,46] To detect the tumors in ABUS images with a CADe system, the suspicious tumor regions in ABUS images were initially segmented. A simple thresholding technique is usually used to segment the tumor region. However, manually selecting an appropriate threshold value is complex because the pixel intensities of the tumors in each case might be different; a fixed threshold value might not be suitable for all cases. In this study, the FCM method was used to classify the pixels of the 3D ABUS image into four classes according to the intensity distribution of each case. The pixels classified in the darkest class were regarded as tumor

Table 1. The Sensitivities of Tumor Detection with a Different Number of Selected Tumor Candidates for Benign and Malignant Tumors.

Number of Selected Tumor Candidates	Benign/Malignant	Sensitivity
5	Total	79.31% (46/58)
	Benign	86.36% (19/22)
	Malignant	75.00% (27/36)
10	Total	86.21% (50/58)
	Benign	90.91% (20/22)
	Malignant	83.33% (30/36)
20	Total	96.55% (56/58)
	Benign	95.45% (21/22)
	Malignant	97.22% (35/36)
30	Total	98.28% (57/58)
	Benign	100.00% (22/22)
	Malignant	97.22% (35/36)

Table 2. The Sensitivities of Tumor Detection with Different Tumor Sizes.

No. of Selected Tumor Candidates	Lesion Size (cm)	Sensitivity
5	<1	70.59% (12/17)
	1-2	85.00% (17/20)
	2-3	55.56% (5/9)
	≥3	100.00% (12/12)
10	<1	82.35% (14/17)
	1-2	90.00% (18/20)
	2-3	66.67% (6/9)
	≥3	100.00% (12/12)
20	<1	88.24% (15/17)
	1-2	100.00% (20/20)
	2-3	100.00% (9/9)
	≥3	100.00% (12/12)
30	<1	94.12% (16/17)
	1-2	100.00% (20/20)
	2-3	100.00% (9/9)
	≥3	100.00% (12/12)

candidate pixels. The threshold value for the tumor segmentation was determined automatically by the FCM method, which eliminates manual variation by using a simple thresholding technique.

After segmenting the suspicious tumor regions, a rule-based method is usually adopted to differentiate the real tumor regions from suspicious tumor regions. However, a manually selected rule might remove some real tumors from the suspicious tumor regions and may also reduce the sensitivity of a CADe system. To prevent these issues, a linear regression model was adopted in this study. The linear regression model automatically estimates the weighting value of each feature with respect to the training data. The estimated weighting value of a feature represents the
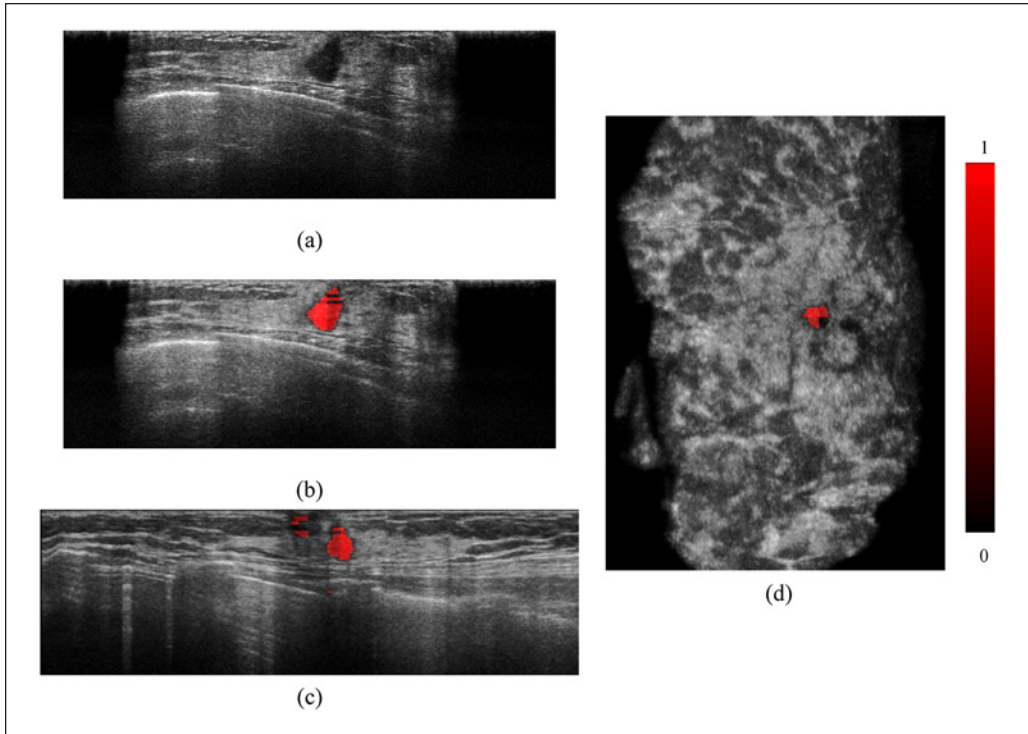
Figure 7. An example of a 1.3-cm infiltrating ductal carcinoma. (a) Transverse view of the original image. (b-d) The detected result in the transverse, longitudinal, and coronal views. The tumor likelihood is represented by a color bar.

importance of differentiating real tumors from suspicious tumor regions and permits the estimation of the tumor likelihoods of suspicious tumor regions.

The sensitivities of the transverse and longitudinal views were greater than that of the coronal view. The differences might be due to the lower resolution in the coronal view. The higher resolutions of the transverse and longitudinal views could improve the sensitivity of tumor detection. When compared with the tumor detection performance in the multiview (using all features), the sensitivity with the multiview was greater than that in the single view. Some lesions may not be readily detected in the single view. Assessing the lesions in each of the three orthogonal views and combining the results could increase lesion detection sensitivity in ABUS images.

The sensitivities of tumor detection using different feature sets were also compared in this article. The tumor detection sensitivity of the morphology feature was lower than the other feature sets. The poor performance of the morphology feature might be attributed to the irregular contour segmentation of tumor candidates. With advanced tumor segmentation, the morphology feature might be useful for tumor detection. The tumor detection sensitivities with the morphology, location, and size features were greater than the sensitivity with only the morphology feature. When N was set to 20 or 30, the sensitivity using the intensity and location size features was slightly higher than that using intensity features alone. This indicates that the location size feature improves the performance of tumor detection. However, to remove rib regions from tumor candidate consideration, the depth feature was also adopted. This may have contributed toward reducing the predicted tumor likelihoods of lesions located proximal to the rib cage.
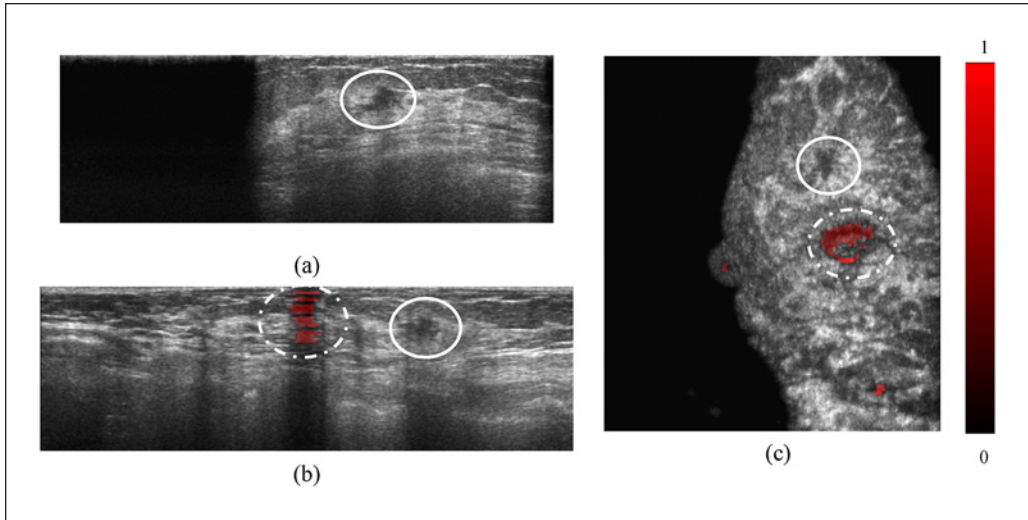
Figure 8. An example of a 0.9 cm infiltrating ductal carcinoma. This case is not detected by the proposed algorithm. (a-c) The detected result in the transverse, longitudinal, and coronal views. The tumor likelihood is represented by the color bar. The solid circle indicates the misdetected lesion and the dash circle indicates the false positive.

For the misdetected lesions, the tumor region was not classified as a tumor candidate region in the FCM stage (see Figure 8). These misdetections occurred because the FCM algorithm is based on pixel intensity. If the intensities of a tumor are bright, the tumor might be not properly segmented with the FCM method. In Figure 9, although the intensities of the lesion are brighter, the difference between the lesion and the surrounding region is significant. If the intensity difference between the suspicious region and the surrounding region is considered in the FCM algorithm, tumor segmentation could be improved.

The proposed method has a higher sensitivity at 98.28% when compared with other studies using the CADe system in ABUS images, which reported sensitivities from 80.6% (3.8 FPs per whole breast image) to 92.3% (1.76 FPs per whole breast image)[13,22]; in addition, there was only one misdetected lesion in our study. The sensitivities of our CADe system were 74.14%, 86.21%, and 94.83% when selecting 3, 10, and 15 tumor candidates, respectively, with the largest likelihoods per pass. Overall, the number of FPs was greater than other studies.[13,22] Most FPs were observed in shadowed areas under the nipple, as indicated by the dashed circle in Figure 8(b) and (c). The intensities of these shadows are similar to those of tumors, which may account for the false reading. Because the shadows under a nipple constitute a linear gradient, morphology features will help to decrease the number of FPs by using better tumor segmentation methods. In addition, the acoustic shadowing feature has been shown to be used to classify different types of tissue well.[47-49] Adopting this feature might improve the performance of a lesion detection system.

Conclusion

Although tumors were able to be detected by our proposed CADe system, the large number of FPs should be reduced before use in clinical diagnoses. Due to poor segmentation used in this study, the morphology features could not accurately differentiate real tumors from suspicious

tumors. In the future, more advanced segmentation could be developed and additional morphology features might improve detection sensitivity and reduce the number of FPs in the CADe system.

References

1. DeSantis C, Siegel R, Bandi P, Jemal A. Breast cancer statistics. CA Cancer J Clin. 2011;61:408-18.
2. Jemal A, Bray F, Center MM, Ferlay J, Ward E, Forman D. Global cancer statistics. CA Cancer J Clin. 2011;61:69-90.
3. Wilson TE, Helvie MA, August DA. Breast cancer in the elderly patient: early detection with mammography. Radiology. 1994;190:203-7.
4. Roubidoux MA, Helvie MA, Lai NE, Paramagul C. Bilateral breast cancer: early detection with mammography. Radiology. 1995;196:427-31.
5. Shapiro S, Venet W, Strax P, Venet L, Roeser R. Ten-to fourteen-year effect of screening on breast cancer mortality. J Natl Cancer Inst. 1982;69:349-55.
6. Kolb TM, Lichy J, Newhouse JH. Comparison of the performance of screening mammography, physical examination, and breast US and evaluation of factors that influence them: an analysis of 27,825 patient evaluations. Radiology. 2002;225:165-75.
7. Boyd NF, Dite GS, Stone J, Gunasekara A, English DR, McCredie MR, et al. Heritability of mammographic density, a risk factor for breast cancer. N Engl J Med. 2002;347:886-94.
8. Boyd NF, Byng JW, Jong RA, Fishell EK, Little LE, Miller AB, et al. Quantitative classification of mammographic densities and breast cancer risk: results from the Canadian National Breast Screening Study. J Natl Cancer Inst. 1995;87:670-5.
9. Boyd NF, Guo H, Martin LJ, Sun L, Stone J, Fishell E, et al. Mammographic density and the risk and detection of breast cancer. N Engl J Med. 2007;356:227-36.
10. Buchberger W, Niehoff A, Obrist P, DeKoekkoek-Doll P, Dunser M. Clinically and mammographically occult breast lesions: detection and classification with high-resolution sonography. Semin Ultrasound CT MR. 2000;21:325-36.
11. Gordon PB, Goldenberg SL. Malignant breast masses detected only by ultrasound. A retrospective review. Cancer. 1995;76:626-30.
12. Berg WA, Blume JD, Cormack JB, Mendelson EB, Lehrer D, Bohm-Velez M, et al. Combined screening with ultrasound and mammography vs mammography alone in women at elevated risk of breast cancer. JAMA. 2008;299:2151-63.
13. Ikedo Y, Fukuoka D, Hara T, Fujita H, Takada E, Endo T, et al. Development of a fully automatic scheme for detection of masses in whole breast ultrasound images. Med Phys. 2007;34:4378-88.
14. Kelly KM, Dean J, Comulada WS, Lee SJ. Breast cancer detection using automated whole breast ultrasound and mammography in radiographically dense breasts. Eur Radiol. 2010;20:734-42.
15. Crystal P, Strano SD, Shcharynski S, Koretz MJ. Using sonography to screen women with mammographically dense breasts. AJR Am J Roentgenol. 2003;181:177-82.
16. Kaplan SS. Clinical utility of bilateral whole-breast US in the evaluation of women with dense breast tissue. Radiology. 2001;221:641-9.

17. Chang RF, Chang-Chien KC, Chen HJ, Chen DR, Takada E, Moon WK. Whole breast computer-aided screening using free-hand ultrasound. International Congress Series. 2005;1281:1075-80.

18. Chou YH, Tiu CM, Chen J, Chang RF. Automated full-field breast ultrasonography: the past and the present. J Med Ultrasound. 2007;15:31-44.

19. Moon WK, Shen YW, Huang CS, Chiang LR, Chang RF. Computer-aided diagnosis for the classification of breast masses in automated whole breast ultrasound images. Ultrasound Med Biol. 2011;37:539-48.

20. Tozaki M, Isobe S, Yamaguchi M, Ogawa Y, Kohara M, Joo C, et al. Optimal scanning technique to cover the whole breast using an automated breast volume scanner. Jpn J Radiol. 2010;28:325-8.

21. Shin HJ, Kim HH, Cha JH, Park JH, Lee KE, Kim JH. Automated ultrasound of the breast for diagnosis: interobserver agreement on lesion detection and characterization. AJR Am J Roentgenol. 2011;197:747-54.

22. Chang RF, Chang-Chien KC, Takada E, Huang CS, Chou YH, Kuo CM, et al. Rapid image stitching and computer-aided detection for multipass automated breast ultrasound. Med Phys. 2010;37:2063-73.

23. Bezdek JC, Ehrlich R, Full W. FCM - the fuzzy C-means clustering-algorithm. Comput Geosci. 1984;10:191-203.

24. Clark MC, Hall LO, Goldgof DB, Clarke LP, Velthuizen RP, Silbiger MS. MRI segmentation using fuzzy clustering-techniques. IEEE Eng Med Biol Mag. 1994;13:730-42.

25. Chen W, Giger ML, Bick U. A fuzzy C-means (FCM)-based approach for computerized segmentation of breast lesions in dynamic contrast-enhanced MR images. Acad Radiol. 2006;13:63-72.

26. Sookpotharom S. Border detection of skin lesion images based on fuzzy C-means thresholding. In: Proceedings of the 2009 3rd International Conference on Genetic and Evolutionary Computing, Guilin, People's Republic of China, 14-17 October; 2009, IEEE, pp.777-80.

27. Hosmer D, Lemeshow S. Applied Logistic Regression (Wiley Series in Probability and Statistics). New York: Wiley Interscience; 2000.

28. Liberman L, Menell JH. Breast Imaging Reporting and Data System (BI-RADS). Radiol Clin North Am. 2002;40:409-30.v.

29. Lee J-S. Digital image smoothing and the sigma filter. Comput Vis Graph Image Process. 1983;24:255-69.

30. Czerwinski RN, Jones DL, O'Brien WD Jr. Line and boundary detection in speckle images. IEEE Trans Image Process. 1998;7:1700-14.

31. Czerwinski RN, Jones DL, O'Brien WD Jr. Detection of lines and boundaries in speckle images-application to medical ultrasound. IEEE Trans Med Imaging. 1999;18:126-36.

32. Rakotomamonjy A, Deforge P, Marche P. Wavelet-based speckle noise reduction in ultrasound B-scan images. Ultrason Imaging. 2000;22:73-94.

33. Marom E, Kresic-Juric S, Bergstein L. Speckle noise in bar-code scanning systems–power spectral density and SNR. Appl Opt. 2003;42:161-74.

34. Abd-Elmoniem KZ, Youssef ABM, Kadah YM. Real-time speckle reduction and coherence enhancement in ultrasound imaging via nonlinear anisotropic diffusion. IEEE Trans Biomed Eng. 2002;49:997-1014.

35. Giger ML, Al Hallaq H, Huo Z, Moran C, Wolverton DE, Chan CW, et al. Computerized analysis of lesions in US images of the breast. Acad Radiol. 1999;6:665-74.

36. Horsch K, Giger ML, Vyborny CJ, Venta LA. Performance of computer-aided diagnosis in the interpretation of lesions on breast sonography. Acad Radiol. 2004;11:272-80.

37. Gonzalez RC, Woods RE. Digital Image Processing. Reading, MA: Addison-Wesley; 1992.

38. Tang H, Zhuang T, Wu EX. Realizations of fast 2-D/3-D image filtering and enhancement. IEEE Trans Med Imaging. 2001;20:132-40.

39. Watson L. The role of ultrasound in breast imaging. Radiol Technol. 2000;71:441-59. quiz 460-2.

40. Dillencourt MB, Samet H, Tamminen M. A general approach to connected-component labeling for arbitrary image representations. J ACM. 1992;39:253-80.

41. Shen WC, Chang RF, Moon WK. Computer aided classification system for breast ultrasound based on Breast Imaging Reporting and Data System (BI-RADS). Ultrasound Med Biol. 2007;33:1688-98.

42. Bribiesca E. An easy measure of compactness for 2D and 3D shapes. Pattern Recogn. 2008;41:543-54.

43. Kohavi R, John GH. Wrappers for feature subset selection. Artif Intell. 1997;97:273-324.
44. Picard RR, Cook RD. Cross-validation of regression models. J Am Stat Assoc. 1984;79:575-83.
45. Chakraborty DP, Breatnach ES, Yester MV, Soto B, Barnes GT, Fraser RG. Digital and conventional
     chest imaging: a modified ROC study of observer performance using simulated nodules. Radiology.
     1986;158:35-9.
46. Sahiner B, Chan HP, Hadjiiski LM, Roubidoux MA, Paramagul C, Bailey JE, et al. Multi-modality
     CADx: ROC study of the effect on radiologists' accuracy in characterizing breast masses on mammo-
     grams and 3D ultrasound images. Acad Radiol. 2009;16:810-8.
47. Drukker K, Giger ML, Mendelson EB. Computerized analysis of shadowing on breast ultrasound for
     improved lesion detection. Med Phys. 2003;30:1833-42.
48. Drukker K, Giger ML, Horsch K, Kupinski MA, Vyborny CJ, Mendelson EB. Computerized lesion
     detection on breast ultrasound. Med Phys. 2002;29:1438-46.
49. Madabhushi A, Peng Y, Rosen M, Weinstein S. Distinguishing lesions from posterior acoustic shadow-
     ing in breast ultrasound via non-linear dimensionality reduction. Conf Proc IEEE Eng Med Biol Soc.
     2006;1:3070-3.